Single nucleus RNA-sequencing reveals altered intercellular communication and dendritic cell activation in nonobstructive hypertrophic cardiomyopathy

Christina J. Codden[1], Amy Larson[1], Junya Awata[1], Gayani Perera[1] and Michael T. Chin[1,2,*]

[1]Molecular Cardiology Research Institute, Tufts Medical Center, Boston, MA, USA

[2]Hypertrophic Cardiomyopathy Center, Tufts Medical Center, Boston, MA, USA

*To whom correspondence should be addressed

Michael T. Chin, MD, PhD

Molecular Cardiology Research Institute

Tufts Medical Center

800 Washington Street, Box 80

Boston, MA 02111

T: 617 636 8776

F: 617 636 5999

The authors have declared that no conflict of interest exists.

Abstract

End stage, nonobstructive hypertrophic cardiomyopathy (HCM) is an intractable condition with no disease-specific therapies. To gain insights into the pathogenesis of nonobstructive HCM, we performed single nucleus RNA-sequencing (snRNA-seq) on human HCM hearts explanted at the time of cardiac transplantation and organ donor hearts serving as controls. Differential gene expression analysis revealed 64 differentially expressed genes linked to specific cell types and molecular functions. Analysis of ligand-receptor pair gene expression to delineate potential intercellular communication revealed significant reductions in expressed ligand-receptor pairs affecting the extracellular matrix, growth factor binding, peptidase regulator activity, platelet-derived growth factor binding and protease binding in the HCM tissue. Changes in Integrin-β1 receptor expression were responsible for many changes related to extracellular matrix interactions, by increasing in dendritic, smooth muscle and pericyte cells while decreasing in endothelial and fibroblast cells, suggesting potential mechanisms for fibrosis and microvascular disease in HCM and a potential role for dendritic cells. In contrast, there was an increase in ligand-receptor pair expression associated with adenylate cyclase binding, calcium channel molecular functions, channel inhibitor activity, ion channel inhibitor activity, phosphatase activator activity, protein kinase activator activity and titin binding, suggesting important shifts in various signaling cascades in nonobstructive, end stage HCM.

Brief summary

End stage, nonobstructive human HCM is associated with altered intercellular communication and dendritic cell activation, providing novel insights into potential disease mechanisms.

45 **Introduction**

46

47 Hypertrophic Cardiomyopathy (HCM) is an inherited disorder characterized by unexplained left
48 ventricular hypertrophy, often asymmetric, often involving the interventricular septum, often
49 associated with left ventricular outflow tract (LVOT) obstruction, fibrosis, microvascular
50 occlusion, and sudden cardiac death. Genetic studies have identified numerous causal
51 mutations in a variety of sarcomere genes such as *MYH7*, *MYL2, MYL3*, *MYBPC3*, *TNNT2*, *TNNI3*
52 and *TPM1*, leading to the concept that HCM is a disease of the sarcomere [1], but genetic testing
53 is only informative in approximately 30% of probands, indicating that other genes and factors
54 significantly contribute to the HCM phenotype. Recently, it has been recognized that in most
55 cases HCM can be considered polygenic with multiple loci contributing to the phenotype or in
56 some cases acting as modifiers of existing sarcomere mutations, by affecting modifiable risk
57 factors such as diastolic blood pressure [2-4]. Patients with sarcomere gene mutations have been
58 found to have more adverse events than those without sarcomere mutations [5], thus implicating
59 a need for better understanding of distinct pathogenic steps in these two groups. The
60 development of fibrosis is associated with an increased risk of sudden cardiac death and is a
61 poor prognostic factor [6-11]. Excess deposition of extracellular matrix (ECM) proteins can cause
62 cardiac stiffening, which can impede contraction [6]. It can additionally disrupt electrical coupling,
63 heightening patient susceptibility to arrhythmogenesis. In the end-stages of disease, fibrosis
64 replaces up to 50% of the myocardium and is a key determinant of patient outcome [9-11].

65

66 Although LVOT obstruction is common and easily treatable in HCM, a subset of patients with
67 nonobstructive HCM develop progressive, symptomatic heart failure, despite guideline directed
68 medical therapy, often leading to heart transplantation [12]. Histopathological features include
69 myocyte hypertrophy, fibrosis, myocyte disarray and microvascular disease and are common
70 with obstructive HCM. The genetic profiles of patients with nonobstructive HCM are also
71 indistinguishable from those with obstructive HCM, raising questions about the sources of
72 asymmetric hypertrophy. Human tissue for study of nonobstructive HCM can only be obtained
73 postmortem or at the time of heart transplantation or other cardiac procedure.
74
75 Single cell and single nucleus transcriptomic analysis have facilitated an understanding of
76 cellular phenotypes and interactions occurring in complex tissues such as the heart and high
77 quality datasets of the normal human heart have been published [13-15]. We have recently
78 performed single nucleus RNA-seq analysis of obstructive HCM and found significant alterations
79 in intercellular communication pathways that affect the extracellular matrix, involving integrin-
80 β1, thus providing a potential mechanism linking sarcomere dysfunction to extracellular matrix
81 signaling [16]. Here, we analyze single nucleus transcriptomes in tissue from nonobstructive, end
82 stage HCM and compare with normal tissue. As with obstructive HCM, we find that alterations
83 in intercellular communication pathways affecting the extracellular matrix involve integrin-β1,
84 but there are additional alterations in communication between fibroblasts, vascular cells, and
85 dendritic cells not seen in obstructive HCM. In addition, there are increases in various molecular
86 functions associated with adenylate cyclase signaling, ion channel function, protein
87 phosphatase and protein kinase activity, suggesting a unique intercellular signaling milieu

88 specific to nonobstructive HCM. These findings have important implications for the
89 development of novel therapies for nonobstructive HCM.
90
91 **Results**
92 **Patient characteristics**
93 Explanted heart tissue was obtained from six HCM patients with severely symptomatic,
94 nonobstructive, end stage disease who underwent cardiac transplantation. Patient
95 characteristics are summarized in Table 1. Patients gave informed consent for their heart tissue
96 to be used in research. The patients varied in age from 25 to 67. Five of six patients were
97 female. Two of the patients carried pathogenic MYH7 mutations and the remaining four
98 patients had no known mutations pathogenic for HCM. Four organ donors and datasets for the
99 normal human IVS have been previously described [15] and are summarized in Table 2 with the
100 two additional donors used in this study.
101
102 **Nonobstructive HCM IVS tissue reveals extensive cardiomyocyte and fibroblast diversity**
103 After sequencing and initial data processing with Cell Ranger software [17], each sample dataset
104 was processed further to remove called nuclei that were likely droplets with ambient RNA, or
105 droplets that contained two nuclei. The six HCM datasets and six donor heart datasets were
106 combined into one dataset using the Seurat Integration function [18]. The final combined dataset
107 included 49010 nuclei from nonobstructive HCM hearts and 34358 nuclei from donor hearts.
108 Clustering of the integrated dataset revealed 22 cell populations within the IVS which was
109 visualized using the dimensionality reduction algorithm uniform manifold approximation and

110 projection (UMAP, Fig. 1A). Each point represents a single nucleus colored by cluster identity.
111 Visualizing the integrated dataset by Normal and HCM datasets reveals that all 22 clusters are
112 present in each condition and all samples contribute to all clusters (Fig. 1B, C, D). No cell
113 populations (i.e., clusters) were specific to either condition.
114
115 Cell identities were assigned to each cluster using known gene markers of expected cell types,
116 differentially expressed genes queried against panglaoDB [19], gene ontology (GO) using GOstats
117 [20], and Ingenuity Pathway Analysis [21]. Supplemental Table 1 lists the gene markers used to
118 identify each cell type. Supplemental Table 2 lists the consensus cell identity assignment using
119 all four methods. Upon assigning cell types, we found that similar cell types expressed similar
120 markers and the associated clusters were expectedly positioned close to each other in UMAP
121 space (Fig. 2A, B). Interestingly, we see ten cardiomyocyte populations (i.e., clusters) and six
122 fibroblast populations, revealing significant cardiomyocyte and fibroblast diversity in the IVS
123 (Fig. 2A, 2B), consistent with previous reports [15, 16]. Other cell types identified included
124 endothelial, smooth muscle, pericyte, neuronal, leukocyte, and dendritic cell populations.
125 Among normal donor heart samples, assigned cardiomyocytes made up approximately 48.5% of
126 the total cell population. Similarly, among nonobstructive HCM samples cardiomyocytes made
127 up approximately 55.0% of the total cell population. Noncardiomyocytes make up the
128 remaining cell population. Nonobstructive HCM does not appear to be associated with a shift in
129 the relative proportion of cells in the heart.
130

131 **Trajectory analysis and differential gene expression analysis reveal nonobstructive HCM-**
132 **associated perturbations**
133 Clustering analysis revealed diversity of both cardiomyocytes and fibroblasts. To gain insight
134 into the potential relationships among the different cell populations for each cell type, clusters
135 were projected onto pseudotime trajectory analysis using Monocle3 [22]. Trajectory analysis was
136 performed on Normal cells only, nonobstructive HCM cells only, and both conditions combined
137 for each of the 8 cell types identified in the above analysis. In single-cell trajectory analysis, a
138 trajectory is a computed path that describes a cell type's biological progression through a
139 dynamic process. Prior to building trajectory paths, the root node, or beginning, of each
140 trajectory path was determined through hierarchical clustering of our single nuclei data by cell
141 type. Then, trajectory paths for each assigned cell type (assigned in Seurat) were constructed in
142 UMAP space using Monocle3 with Normal and HCM data together and individually. Once
143 trajectory paths were established, pseudotime could be assigned to each cell. For all cell types,
144 root nodes showed consistent placement among Normal only groups, HCM only groups, and
145 Normal and HCM groups. Trajectory paths also showed similar basic structures among Normal
146 only groups, HCM only groups, and Normal and HCM group (data not shown). Therefore, we
147 were not able to distinguish any meaningful changes among trajectory paths. These findings
148 suggest that the relationships between the various subtypes of each cell type do not vary
149 significantly in nonobstructive HCM heart tissue in comparison to Normal heart tissue, as we
150 have reported for obstructive HCM [16].
151

152 Establishment of trajectories facilitates the analysis of differential gene expression along the
153 trajectory and between conditions along the trajectory. We analyzed differential gene
154 expression for each cell type along their trajectories for the Normal and HCM populations.
155 Differential expression analysis between Normal and HCM cells by assigned cell type and cluster
156 was performed in which generalized linear regression models were fit for each gene. Resulting
157 coefficients were tested for significant differences from zero, with an adjusted p-value cutoff
158 ≤0.05 using the Wald Test. No differentially expressed genes were detected by this method.
159
160 Differential gene expression can also be analyzed along trajectory paths in UMAP space through
161 spatial autocorrelation. Moran's I statistic and adjusted p-values were calculated for each gene
162 in Normal only and HCM only groups within each cell type. When paired with a significant p-
163 value (≤0.05), a Moran's I statistic value near zero indicated no spatial autocorrelation and a
164 value near 1 indicated perfect positive autocorrelation in which a gene is expressed in a focal
165 region of the UMAP space. Results showed between 115 and 6695 genes are differentially
166 expressed along trajectory paths among cell types and between 18 and 4518 differentially
167 expressed genes overlapped between Normal and HCM groups among cell types (Supplemental
168 Table 3).
169
170 Since many genes showed differential expression over UMAP space, further conservative
171 filtering was performed to identify genes of interest. Genes with Moran's I statistic available for
172 a single condition, Normal or HCM, were filtered by a Moran's I statistic value above 0.1, while
173 genes with Moran's I statistics available for both classes were filtered by an absolute difference

174 >0.1. For each cell type, 1 to 18 genes passed the filter with 64 unique genes in total passing the
175 filter among all cell types (Supplemental Table 4). The expression of these filtered genes was
176 then plotted in UMAP space for their associated cell type in Normal and HCM conditions as
177 shown for a subset of identified genes in cardiomyocytes (Supplemental Figure 1). Visual
178 analysis of the UMAP plots revealed 44 genes with pronounced differences in their spatial
179 expression between Normal and nonobstructive HCM conditions (summary in Table 3). Of these
180 44 genes, 3 (*MYH7, MYL2, TNNT2*) are already known to be associated with human HCM. GO
181 Enrichment analysis of these 44 differentially expressed genes revealed significant enrichment
182 for molecular functions involving actin binding, biological processes involving muscle
183 development and muscle differentiation and cellular components including the sarcomere,
184 myofibril and contractile fiber (Fig. 3A). Analysis of genes from this list showing increased
185 expression in nonobstructive HCM revealed significant enrichment in molecular functions
186 involving structural constituent of muscle and actin binding, no enriched biological processes
187 and enrichment in cellular components involving the sarcomere, myofibril and contractile fiber
188 (Fig. 3B). Analysis of genes from this list showing decreased expression in nonobstructive HCM
189 revealed enrichment for molecular functions involving lipid transport and the ECM structural
190 constituent, biological processes involving muscle differentiation, muscle development, lipid
191 transport and lipid localization, and cellular components involving the endoplasmic reticulum
192 membrane (Fig. 3C).
193
194 **Ligand-receptor pair gene expression indicates alteration of intercellular communication in**
195 **HCM**

196 *HCM is associated with a general decrease in cell-cell communication but an increase in*
197 *fibroblast, smooth muscle cell and pericyte to dendritic communication and an increase in*
198 *smooth muscle cell to leukocyte communication*
199
200 To quantify potential cardiac cell-cell communication in Normal and nonobstructive HCM IVS
201 tissue, we quantified the number of possible expressed ligand-receptor pairs among cell types
202 as previously described [23, 24]. We examined the expression of a curated list of 3627 unique
203 human ligand-receptor (L-R) pairs derived by combining a collection of 2557 human L-R pairs [25]
204 with another set of 3398 human L-R pairs [26] and eliminating duplicate pairs. Ligands and
205 receptors were considered expressed if their associated gene was detectable in ≥ 20% of cells in
206 a cell type. Notably, quantification of cell-cell communication in this study represents potential
207 communication as we account for only expressed ligand-receptor pairs and not the position or
208 boundaries of cell types. Results showed that nonobstructive HCM IVS tissue demonstrated a
209 reduced intercellular communication network among our 8 identified cell types compared to
210 normal IVS tissue (Fig. 4). Quantitatively, the total number of expressed ligand-receptor pairs in
211 the nonobstructive HCM tissue (n=405) was much lower than in Normal tissue (n=710, Fig. 4A,
212 B). Analysis of the broadcast ligands by individual cell types demonstrates that 1) all cells except
213 for smooth muscle cells show a broad decrease in both paracrine and autocrine ligand
214 broadcasting in nonobstructive HCM (Fig. 4B, C, D) and 2) fibroblasts broadcast the greatest
215 number of ligands to the other cell types in both Normal and nonobstructive HCM tissue.
216 Analysis of receptor expression again showed a broad decrease across cell types, except for
217 dendritic cells (Fig. 4B, C, D). Fibroblast communication is particularly high with fibroblast,

218 endothelial, pericyte, smooth muscle, neuronal, and cardiomyocyte cells (Fig. 4). While
219 intercellular communication was generally reduced in nonobstructive HCM tissue compared to
220 Normal tissue, there was several cases of increased nonobstructive HCM communication, from
221 fibroblasts, smooth muscle cells, pericytes and cardiomyocytes to dendritic cells and from
222 smooth muscle cells to leukocytes (Fig 4C, D).
223
224 Communication between fibroblasts and dendritic cells increased from 5 to 13 L-R pairs in
225 nonobstructive HCM tissue due primarily to the dendritic cells in nonobstructive HCM tissue
226 gaining *ITGB1* receptor expression to enable communication with several cognate ligands
227 (COL1A2, COL3A1, COL4A1, COL6A1, COL6A2, COL6A3, FN1, LAMA2, LGALS1, LUM;
228 Supplemental Table 5). The increase in smooth muscle cell to dendritic cell communication (3
229 to 9 L-R pairs) is also primarily due to dendritic cells in nonobstructive HCM tissue gaining *ITGB1*
230 receptor expression, to enable communication with several smooth muscle cell cognate ligands
231 (COL1A2, COL4A1, COL6A1, COL6A2, FN1, LGALS1; Supplemental Table 5). Similarly, increased
232 pericyte to dendritic cell interaction (3 to 8 L-R pairs) is also due primarily to nonobstructive
233 tissue dendritic cells gaining ITGB1 receptor expression, to enable communication with several
234 pericyte cognate ligands (COL1A2, COL4A1, COL6A1, COL6A2, FN1, LGALS1; Supplemental Table
235 5). The increase in smooth muscle cell to leukocyte communication in nonobstructive HCM (6 to
236 10 L-R pairs) is due to leukocytes gaining ITGB1 receptor expression, to enable communication
237 with several smooth muscle cell cognate ligands (COL1A2, COL4A1, COL6A1, COL6A2, FN1)
238 (Supplemental Table 6).
239

240 *Changes in ligand-receptor pair gene expression imply alterations in molecular function*

241

242 To assess the molecular functions potentially affected by changes in ligand-receptor signaling
243 among our 8 identified cell types, GO enrichment analysis was performed on the ligands and
244 receptors in expressed ligand-receptor pairs from both Normal and nonobstructive HCM tissue
245 (Fig. 5). We observed a decrease in most identified ligand molecular functions (34 of 47) in the
246 nonobstructive HCM heart tissue compared to the Normal heart tissue, with complete loss of
247 functions involving insulin receptor binding, insulin-like growth factor receptor binding,
248 lipoprotein particle receptor binding, and structural molecule activity conferring elasticity (note,
249 these are low count normal MFs; Figure 5A). Large decreases in nonobstructive molecular
250 functions relative to Normal (>100 count difference) were found for extracellular matrix
251 structural constituent, extracellular matrix structural constituent conferring tensile strength
252 (56%), growth factor binding (57%), peptidase regulator activity (75%), platelet-derived growth
253 factor binding (56%), protease binding (74%; Figure 5A). Large increases in molecular functions
254 in nonobstructive HCM tissue relative to normal tissue (>50 count difference) were noted for
255 adenylate cyclase binding, calcium channel inhibitor activity, calcium channel regulator activity,
256 channel inhibitor activity, protein kinase activator activity, protein N-terminus binding, protein
257 phosphatase activator activity, protein serine threonine kinase activator activity and titin
258 binding. When ligand molecular function is assessed in individual cell types, a general decrease
259 in most nonobstructive molecular functions is observed compared to the normal condition
260 (Figure 5B-I) with generally more drastic decreases in cardiomyocytes, endothelial cells,
261 dendritic cells, leukocytes, and neuronal cell ligand molecular functions (Figure 5). Less drastic

262 decreases and increases are observed in non-obstructive ligand molecular functions among
263 fibroblasts, pericytes, and smooth muscle cells (Figure 5).
264
265 Molecular functions associated with changes in receptor expression align with changes in ligand
266 expression (Fig. 6A) including the finding of a general decrease in most nonobstructive
267 molecular functions compared to the Normal condition (46 of 65 molecular functions; Figure 6).
268 The largest decreases (>100 count difference) in nonobstructive molecular functions compared
269 to Normal included amyloid beta binding, coreceptor activity, lipoprotein, peptide binding, and
270 scavenger receptor activity (Figure 6A). The largest increases (> 100 count difference) in
271 nonobstructive molecular functions relative to Normal included amide binding, calcium
272 molecular functions, calmodulin binding, channel/gated channel molecular functions, divalent
273 inorganic cation transmembrane transporter activity, metal ion transmembrane transporter
274 activity, protein kinase A activity, and sulfur compound binding (Figure 6A). Trends in receptor
275 molecular functions in individual cell types are notable for increases related to signal
276 transduction in dendritic cells and leukocytes, particularly calcium channel activity and protein
277 kinase A activity in dendritic cells.
278
279 *Fibroblast subtypes show subtype-specific changes in cell-cell communication*
280
281 To better understand the interaction between the different fibroblast populations and other
282 cell types in the IVS, we examined the potential ligand-receptor communication through cell
283 network plots for all fibroblast subtypes alongside the other previously identified 7 cell types

284 (Fig. 7A, C, D). In Normal tissue, all fibroblast subtypes broadcast ligands extensively to
285 generate a dense intercellular network. In nonobstructive HCM tissue, the intercellular
286 communication network for fibroblast subtypes shows a reduced number of broadcasting
287 ligands compared to Normal tissue, (1502 versus 2636 respectively; Fig. 7A, B). Fibroblast
288 cluster 2 generated the highest number of broadcasting ligands in both conditions. The largest
289 decreases in potential interactions occurred between fibroblast cluster 2 and fibroblast clusters
290 2 through 6 (Supplemental Table 7) and between fibroblast cluster 5 and fibroblast clusters 2
291 through 6 (Supplemental Table 8). In fibroblast cluster 2 from nonobstructive HCM tissue, there
292 was a disproportionate reduction in expression of cognate ligands for the ITGB1 receptor
293 (COL18A1, COL5A1, COL5A2, FBLN1, FBN1, HSPG2, LAMC1, LGALS3BP, NID1, THBS2) and also of
294 ligands for the LRP1 receptor (APP, C3, CALR, CTGF, HSPG2, LRPAP1, SERPINE2, SPERPING1,
295 TFPI). *ITGB1* and *LRP1* were expressed in both normal and nonobstructive HCM fibroblasts from
296 cluster 2. Interaction between fibroblast cluster 2 and fibroblast clusters 3-5 was reduced in
297 nonobstructive HCM primarily due to loss of the LRP1 receptor and several cognate ligands for
298 the ITGB1 receptor (COL18A1, COL5A1, COL5A2, FBLN1, FBN1, HSPG2, LAMC1, LGALS3BP, NID1,
299 THBS2). *ITGB1* was expressed in fibroblast clusters 3-5 in both normal and nonobstructive HCM
300 tissue.
301
302 *Cardiomyocyte subtypes show subtype-specific changes in cell-cell communication*
303
304 To better understand the interaction between the different cardiomyocyte populations and
305 other cell types in the IVS, we performed L-R analysis for all ten cardiomyocyte subtypes and

306 the other 7 cell types (Fig. 8). In nonobstructive HCM tissue, there is again a general decrease in
307 intercellular communication (2634 L-R pairs in normal, reduced to 2026 in nonobstructive HCM;
308 Fig. 8A, B), but the degree of reduction is lower than seen when subtypes are not considered or
309 when fibroblast subtypes are considered. The largest decreases occur in ligands broadcast from
310 endothelial cells and in receptors expressed by fibroblasts and the cardiomyocyte 4 cluster.
311 Notably, there are increases in ligands broadcast by cardiomyocyte clusters 1, 2, 5, 9 and by
312 smooth muscle cells and in receptors in cardiomyocyte clusters 1, 3 and 9 and dendritic cells in
313 nonobstructive HCM (Fig. 8B). The greatest reductions in intercellular L-R connections involve
314 fibroblasts broadcasting to fibroblasts and cardiomyocyte cluster 4 (Supplemental Table 9), and
315 from endothelial cells broadcasting to fibroblasts, cardiomyocyte cluster 4 and cardiomyocyte
316 cluster 8 (Supplemental Table 10). In both cases, reduction in intercellular communication is
317 due to loss of LRP1 receptor expression in fibroblasts as well as loss of ligands for ITGB1
318 (COL11A1, FBLN1, FBN1, HSPG2, LAMB1, LAMC1, NID1, VCAN) in fibroblasts and endothelial
319 cells. Notably, *ITGB1* is expressed in fibroblasts and cardiomyocyte clusters 4 and 8 in both
320 Normal tissue and nonobstructive HCM tissue. Increases in communication from cardiomyocyte
321 clusters 2, 5, fibroblasts and smooth muscle cells to cardiomyocyte cluster 9 is due to gain of
322 expression of *ITGB1* in cardiomyocyte cluster 9 (Supplemental Table 11). Increased
323 communication from cardiomyocyte cluster 5 to dendritic cells is also due to gain of expression
324 of *ITGB1* in dendritic cells (Supplemental Table 12).
325
326 *Cardiomyocyte subtypes and fibroblast subtypes together show cell subtype-specific alterations*
327 *in cell-cell communication*

328

329 Given that cardiomyocytes and fibroblasts are the most numerous cells in the heart and
330 demonstrate the most subtypes in our study, we examined the intercellular networks between
331 cardiomyocyte subtypes and fibroblast subtypes in normal tissue and nonobstructive HCM. The
332 total number of expressed ligand-receptor pairs in the Normal tissue was greater than in the
333 nonobstructive HCM tissue (3354 and 2399 expressed ligand-receptor pairs respectively, Fig. 9).
334 The largest decreases in cellular communication involved fibroblast cluster 5, through reduction
335 in both broadcasted ligands and expressed receptors. The largest reductions in L-R pairs
336 occurred between fibroblast clusters 2 or 5 and fibroblast clusters 2-6 (Supplemental Table 13)
337 and resulted from loss of ligands for ITGB1, which was still expressed in the recipient cells in
338 both normal and nonobstructive HCM, or from loss of the LRP1 receptor in recipient fibroblast
339 clusters except for fibroblast cluster 2. The largest increases in communication due to ligand
340 broadcasting involved cardiomyocyte clusters 2, 5 and 9 and increases due to receptor
341 expression involved cardiomyocyte clusters 1, 3, 9 and fibroblast cluster 1 (Fig. 9B). Increased
342 communication to cardiomyocyte cluster 9 from fibroblast clusters 1-5 and cardiomyocyte
343 clusters 2, 3 and 5 were due to gain of ITGB1 expression in cardiomyocyte cluster 9
344 (Supplemental Table 14).

345

346 **Discussion**

347

348 HCM has long been considered a disease of the sarcomere based on the association of
349 sarcomere gene mutations with HCM, but the contributions from other loci are increasingly

350 appreciated [2, 3], as are potential mechanisms aside from sarcomere dysfunction [27]. We have
351 previously examined single nuclei gene expression patterns in obstructive HCM. In this prior
352 study, we did not identify any HCM-specific cell populations but observed a profound reduction
353 in intercellular communication, especially in pathways mediated by ITGB1, and altered
354 extracellular matrix gene expression, which may explain some of the nonmyocyte phenotypes
355 seen in HCM such as fibrosis and link these phenotypes to alterations in mechanical signal
356 transduction [16]. In the current study, we performed a single nucleus transcriptome analysis of
357 tissue from patients with nonobstructive HCM, using tissue from the IVS harvested at the time
358 of cardiac transplantation. This patient population is distinct from those with obstructive HCM
359 in that they do not have LVOT obstruction and generally have more severe, intractable heart
360 failure that results in cardiac transplantation. Determining gene expression patterns at the
361 single cell level in nonobstructive HCM thus has the potential for facilitating precision medicine
362 approaches for this specific population, through overlapping and unique pathogenic
363 mechanisms relative to obstructive HCM.
364
365 The single nuclei gene expression patterns for nonobstructive HCM parallel those for
366 obstructive HCM in that there are no disease-specific cell clusters and there is a reduction in
367 intercellular communication, particularly in pathways involving ITGB1 and its associated ECM
368 ligands. As with obstructive HCM, changes in gene expression involve sarcomere genes known
369 to be associated with HCM and GO analysis indicates that gene expression changes are relevant
370 to the extracellular matrix and sarcomere function, indicating that these are common,
371 fundamental disease processes in HCM, regardless of LVOT obstruction. We have previously

372 noted that a reduction in ECM associated gene expression and molecular function in
373 obstructive HCM is counterintuitive based on the association between HCM and increased
374 fibrosis and have suggested that the reduction in gene expression may represent a negative
375 feedback loop that follows the accumulation of ECM protein in tissue [16]. Concordant findings in
376 nonobstructive HCM can be explained similarly. Precision medicine approaches that target
377 integrin signaling and ECM interaction may one day prove useful for both obstructive and
378 nonobstructive HCM.
379
380 A notable difference between obstructive and nonobstructive HCM in our current study,
381 however, involves the unexpected increases in communication between fibroblasts, smooth
382 muscle cells and pericytes with dendritic cells and between smooth muscle cells and leukocytes
383 in the nonobstructive HCM condition relative to the control condition. Immune cells have been
384 demonstrated to play important roles in development of cardiac hypertrophy and fibrosis in a
385 pressure overload model of rodent hypertrophy (reviewed in [28]). Dendritic cells function as
386 antigen presenting cells that activate T cell responses and depletion of these cells reduces
387 cardiomyocyte hypertrophy, cardiac fibrosis, LV remodeling and inflammatory cell infiltration
388 after pressure overload [29]. A role for dendritic cells in human heart failure is less well-
389 established, although a trend toward elevated numbers in blood has been reported [30]. Integrin-
390 mediated signaling has been shown to be an important determinant of dendritic cell function,
391 with ITGB1 determining dendritic morphology [31] and promoting an anti-inflammatory
392 phenotype in bone-marrow-derived dendritic cells [32]. Our data linking dendritic cells to
393 fibroblasts, smooth muscle cells and pericytes by ITGB1 signaling is novel and suggests an

394 important role for these cells in the pathological hypertrophy, cardiac fibrosis and vascular
395 abnormalities seen in nonobstructive HCM. Our additional novel observation that signal
396 transduction related molecular functions such as calcium channel activity and protein kinase A
397 activity are increased in dendritic cells from nonobstructive HCM hearts also provides additional
398 potential pathways for precision-medicine guided therapy for nonobstructive HCM.
399
400 We have previously noted extensive cardiomyocyte and fibroblast diversity in the human IVS,
401 likely due to the diverse origins of the cells within this anatomic region [15, 16]. We have also
402 noted that the different cardiomyocyte and fibroblast subtypes exhibit specific intercellular
403 communication profiles [16, 24] and the phenomenon is observed again in this study. Specific
404 cardiomyocyte and fibroblast subtypes appear to adopt distinct functional roles relevant to the
405 disease process by shifting patterns of gene expression to increase or decrease interactions of
406 cell types. An ongoing challenge is to determine which of these shifts is most relevant to the
407 disease process and thus identify potential therapeutic targets. Future spatial transcriptomic
408 experiments assigning single cell populations to anatomic pathological features of HCM, such as
409 areas of myocyte disarray, fibrosis, focal myocyte hypertrophy, and vascular abnormalities will
410 likely be informative. Our study is the first to characterize transcription patterns in
411 nonobstructive HCM at single cell resolution and provides an important resource for future
412 investigation of the complex cellular interplay in nonobstructive HCM.
413
414
415 **Methods**

416

417 *Study Patients, Sample Collection and Processing*

418

419 A total of 6 patients with end stage, nonobstructive HCM scheduled for cardiac transplantation
420 were approached for written informed consent to allow their tissue to be used for research.
421 Those who consented underwent surgery and tissue was collected. Explanted heart tissue
422 sample processing was done as previously described [15, 16]. 100 mg of collected interventricular
423 septum tissue was minced into 1 mm^3 pieces, placed in 0.5 mL of CryoStor CS10 Freeze Media
424 (STEMCELL Technologies), and stored in a MrFrosty (ThermoFisher) at 4°C for 10 minutes and
425 then transferred to -80°C overnight. Bulk RNA was isolated from a piece of tissue using the
426 Qiagen RNeasy Plus Micro kit and then assessed on the Agilent Bioanalyzer 2100. Samples with
427 an RNA Integrity Number greater than 8.5 were used in library preparation. Sample collection
428 was approved by the Tufts University/Medical Center Health Sciences Institutional Review
429 Board under IRB protocol # 9487. Patient characteristics were obtained from the medical
430 record and are shown in Table 1. Tissue from organ donor patients without underlying cardiac
431 disease was obtained and processed as described previously [15].

432

433 *Nuclei isolation, library preparation, and sequencing*

434

435 Generation of single nuclei sequencing libraries was performed as previously described [15, 16].
436 Cryopreserved samples were thawed at 37°C and placed on ice. Nuclei were isolated via
437 Dounce homogenization as previously described [33]. Homogenates were filtered through a

438 Pluristrainer 10 µM cell strainer (Fisher Scientific) into a pre-chilled tube. Nuclei were pelleted
439 by centrifuging at 500 x g for 5 min at 4°C. Nuclei pellets were washed and pelleted according to
440 manufacturer protocol (10x Genomics). Nuclei were stained with trypan blue and counted on a
441 hemocytometer to determine concentration prior to loading of the 10x Chromium device and
442 samples were diluted to capture ~10,000 nuclei. Nuclei were separated into Gel Bead Emulsion
443 droplets using the 10x Chromium device according to the manufacturer protocol (10x
444 Genomics). Sequencing libraries were prepared using the Chromium Single Cell 3´ reagent V2
445 kit according to manufacturer's protocol. Libraries were multiplexed and sequenced on a
446 NovaSeq S4 (Illumina) to produce ~50,000 reads per nucleus. Single nuclei RNAseq data for
447 normal IVS tissue from 4 donors is available in the Gene Expression Omnibus database under
448 accession number GSE161921 [15]. Data for nonobstructive HCM IVS tissue and additional normal
449 heart donors is available under accession number GSE181764.
450
451 *Clustering of Cells by Gene Expression Pattern and Assignment of Cell Type Identity*
452
453 Clustering of cells and assignment of cell identity was done as previously described [15, 16].
454 Sequencing reads were processed using Cell Ranger version 6.0.1 [17]. The gene expression matrix
455 was subset to only include reads from the nuclear genome. Quality control (QC) filtering,
456 clustering, dimensionality reduction, visualization, and differential gene expression were
457 performed using the R package Seurat version 3.0. Each dataset was filtered so that genes that
458 were expressed in three nuclei or more were included in the final dataset. The dataset was
459 further sublet to exclude nuclei that had fewer than 200 genes expressed to remove droplets

460 containing only ambient RNA, and to exclude nuclei with greater than 2000 genes to remove
461 droplets that contained two nuclei. Datasets were individually normalized and integrated using
462 Seurat's SCTransform development workflow to reduce batch effects [18]. Optimal clustering
463 resolution was determined using Clustree version 0.4.3 [34] to identify the resolution where the
464 number of clusters stays stable and was determined to be 0.9 for the integrated dataset.
465 Assignment of cell identity to each cluster was performed using four separate analyses.
466 Expression of known cell-specific gene markers were used to identify major cell types, as done
467 previously [13, 15, 24, 35]. The top 20-30 differentially expressed genes in each cluster were also
468 compared with cell type gene expression markers from the PanglaoDB database
469 https://panglaodb.se [19] to independently assign cell type. Entire sets of differentially expressed
470 genes for each cluster were also subjected to Ingenuity Pathway Analysis [21] and their inferred
471 functions were used to identify cluster cell types independently. Upregulated genes from each
472 cluster were also subject to Gene Ontology biological process association using GoStats [20] and
473 these associations were used to refine cell type assignment further.
474
475 *Trajectory Analysis and Identification of Differentially Expressed Genes*
476
477 Trajectory analysis was performed using Monocle3 [22] to determine the relationship between
478 subtypes of cells identified in our clustering analysis as previously described [16]. Since our data
479 do not represent a developmental time course, we determined the root nodes for each subtype
480 by hierarchical clustering prior to generating trajectories and assigning pseudotime to each cell.
481 Each cell type was analyzed in three cohorts: 1. Normal and nonobstructive HCM cells together;

482 2. Normal cells alone; 3. Nonobstructive HCM cells alone. Once trajectories were established,
483 differential expression between Normal and HCM cells by cell type and cluster was performed
484 by fitting a generalized linear regression model to each gene according to the formula $\log(y_i) =$
485 $\beta_0 + \beta_t x_t$. The coefficients β_0 and β_t were extracted from each model and tested for significant
486 difference from zero using the Wald test, which assesses constraints on statistical parameters
487 based on the weighted distance between the unrestricted estimate and its hypothesized value
488 under the null hypothesis, where the weight is the precision of the estimate. A gene was
489 determined to be differentially expressed between Normal and HCM conditions in a cell type or
490 cluster if the Wald test produced an adjusted p-value ≤ 0.05.
491
492 Differentially expressed genes over trajectory paths in UMAP space (i.e., spatial
493 autocorrelation) was performed in Monocle3 using Moran's I statistic. Moran's I statistic is a
494 value that varies from -1 to 1, where -1 indicates perfect dispersion, 0 indicates no spatial
495 autocorrelation, and 1 indicates perfect positive autocorrelation (i.e., nearby cells in have
496 similar gene expression values in focal region of UMAP space). For each Normal and
497 nonobstructive HCM cell type, a gene was determined to be differentially expressed over space
498 if the associated Moran's I statistic value was positive, paired with a significant adjusted p-value
499 ≤ 0.05, and expressed in $\geq 1\%$ of associated cells. Since many genes showed differential
500 expression over space, further conservative filtering was performed in which genes with
501 Moran's I statistic available in a single class (i.e., Normal or HCM) were filtered by Moran's I
502 statistic values >0.1. For genes with Moran's I statistics available in both classes (i.e., Normal
503 and HCM), genes were filtered by an absolute difference >0.1. GO analysis of molecular

504 function and biological process associated with differentially expressed genes was done using
505 the online tools at uniprot.org/uniprotkb [36].
506
507 *Analysis of Ligand-Receptor Pair Gene Expression to Discover Intercellular Communication*
508 *Pathways*
509
510 To quantify potential cardiac cell-cell communication in Normal and HCM hearts, cell
511 communication networks were plotted in igraph version 1.2.6 [37] and compared on the basis of
512 ligand-receptor pair gene expression. Our cell-cell communication networks were derived as
513 described previously [23], using a list of 2557 human ligand-receptor pairs [25] combined with
514 another list of 3398 human ligand-receptor pairs [26], to give a total of 3627 unique human
515 ligand-receptor pairs, largely as described previously [16]. A ligand or receptor for each cell type
516 or cluster was considered expressed if the corresponding gene showed an above zero gene
517 count in ≥ 20% of cells in our snRNAseq data. We initially analyzed the potential signaling
518 interactions between the 8 cell types identified in our snRNAseq data. Lines in our cell networks
519 connect two cell types and represent expressed human ligand-receptor pairs (i.e., potential cell-
520 cell communication between a broadcasting (ligand) and recipient (receptor) cell types. Line
521 color in our networks represents the broadcasting ligand source. Line thickness is proportional
522 to the number of uniquely expressed ligand-receptor pairs. Cell-cell communication networks
523 were also analyzed by fibroblast cluster along with other cell types, by cardiomyocyte cluster
524 and other cell types and by fibroblast clusters and cardiomyocyte clusters. GO analysis of

525 differentially expressed ligand receptor pairs was performed using the R package clusterProfiler
526 [38].
527
528 *Statistics*
529 We used mixed effects models to analyze cell type specific differential expression, while taking
530 into account the variability between and within subjects. A sample size of 6 cases and 6
531 controls, with an average of 3,000 cells per subject, will provide 80% power to detect fold
532 change of expression ranging between 1.3 for an intracluster correlation f 0.01, and 2 for an
533 intracluster correlation of 0.1. The power calculations were pretty stable for sample sizes
534 ranging between 500 and 3000 cells per subject. We used a Bonferroni correction for 10,000
535 tests to fix the level of significance. The power calculations were conducted using Power
536 Analysis and Sample Size software (PASS).
537
538 Other statistical methods to cluster cells in UMAP space and control for batch effects using the
539 built-in functionality of Seurat [18], to determine cluster stability by Clustree [34] and to perform
540 Gene Ontology Analysis using well documented software programs [38] are described in above
541 methods sections and in cited references. Statistical methods to compare gene expression
542 along pseudotime trajectories using linear regression or spatial autocorrelation using the built-
543 in functionality of Monocle3 are described above and in the original cited reference [22].
544
545 *Study Approval*

546 Explanted HCM heart sample collection was approved by the Tufts University/Medical Center
547 Health Sciences Institutional Review Board under IRB protocol # 9487. All subjects gave their
548 informed consent for inclusion before they participated in the study. The study was conducted
549 in accordance with the Declaration of Helsinki. Unused donor hearts were obtained in
550 deidentified fashion from New England Donor Services under a Tufts University/Medical Center
551 Health Sciences IRB approved research protocol after being designated as not human subjects
552 research.
553

554 **Author contributions:**

555 Conceptualization: MTC

556 Data Curation: CJC, AL, GP, MTC

557 Formal Analysis: CJC, MTC

558 Methodology: CJC, AL, JA, GP, MTC

559 Investigation: AL, CJC, JA, GP, MTC

560 Visualization: CJC, AL, MTC

561 Funding acquisition: MTC, AL

562 Project administration: MTC

563 Resources: AL, MTC

564 Software: AL, CJC

565 Supervision: MTC

566 Writing – original draft: MTC

567 Writing – review & editing: AL, CJC, JA, GP, MTC

568

569 **Acknowledgements**

570 We thank Paola Sebastiani for helpful discussions regarding statistics.

571

572 **Funding:**

573 American Heart Association Innovative Project Award 18IPA34170294 (MTC)

574

575 National Center for Advancing Translational Sciences, National Institutes of Health, Award
576 Number UL1TR002544 (MTC)
577
578 National Heart, Lung, and Blood Institute of the National Institutes of Health, Award Number
579 F32HL147492 (AL)
580
581 Beals Goodfellow Award for CardioVascular Research at Tufts Medical Center (AL)
582
583
584
585

586 **References**

587

588 1. Thierfelder L, Watkins H, MacRae C, Lamas R, McKenna W, Vosberg HP, Seidman JG and
589 Seidman CE. Alpha-tropomyosin and cardiac troponin T mutations cause familial hypertrophic
590 cardiomyopathy: a disease of the sarcomere. *Cell*. 1994;77:701-12.
591 2. Harper AR, Goel A, Grace C, Thomson KL, Petersen SE, Xu X, Waring A, Ormondroyd E,
592 Kramer CM, Ho CY, Neubauer S, Investigators H, Tadros R, Ware JS, Bezzina CR, Farrall M and
593 Watkins H. Common genetic variants and modifiable risk factors underpin hypertrophic
594 cardiomyopathy susceptibility and expressivity. *Nat Genet*. 2021;53:135-142.
595 3. Tadros R, Francis C, Xu X, Vermeer AMC, Harper AR, Huurman R, Kelu Bisabu K, Walsh R,
596 Hoorntje ET, Te Rijdt WP, Buchan RJ, van Velzen HG, van Slegtenhorst MA, Vermeulen JM,
597 Offerhaus JA, Bai W, de Marvao A, Lahrouchi N, Beekman L, Karper JC, Veldink JH, Kayvanpour
598 E, Pantazis A, Baksi AJ, Whiffin N, Mazzarotto F, Sloane G, Suzuki H, Schneider-Luftman D, Elliott
599 P, Richard P, Ader F, Villard E, Lichtner P, Meitinger T, Tanck MWT, van Tintelen JP, Thain A,
600 McCarty D, Hegele RA, Roberts JD, Amyot J, Dube MP, Cadrin-Tourigny J, Giraldeau G, L'Allier
601 PL, Garceau P, Tardif JC, Boekholdt SM, Lumbers RT, Asselbergs FW, Barton PJR, Cook SA,
602 Prasad SK, O'Regan DP, van der Velden J, Verweij KJH, Talajic M, Lettre G, Pinto YM, Meder B,
603 Charron P, de Boer RA, Christiaans I, Michels M, Wilde AAM, Watkins H, Matthews PM, Ware JS
604 and Bezzina CR. Shared genetic pathways contribute to risk of hypertrophic and dilated
605 cardiomyopathies with opposite directions of effect. *Nat Genet*. 2021;53:128-134.
606 4. Watkins H. Time to Think Differently About Sarcomere-Negative Hypertrophic
607 Cardiomyopathy. *Circulation*. 2021;143:2415-2417.
608 5. Ho CY, Day SM, Ashley EA, Michels M, Pereira AC, Jacoby D, Cirino AL, Fox JC, Lakdawala
609 NK, Ware JS, Caleshu CA, Helms AS, Colan SD, Girolami F, Cecchi F, Seidman CE, Sajeev G,
610 Signorovitch J, Green EM and Olivotto I. Genotype and Lifetime Burden of Disease in
611 Hypertrophic Cardiomyopathy: Insights from the Sarcomeric Human Cardiomyopathy Registry
612 (SHaRe). *Circulation*. 2018;138:1387-1398.
613 6. Kong P, Christia P and Frangogiannis NG. The pathogenesis of cardiac fibrosis. *Cell Mol*
614 *Life Sci*. 2014;71:549-74.
615 7. Ma ZG, Yuan YP, Wu HM, Zhang X and Tang QZ. Cardiac fibrosis: new insights into the
616 pathogenesis. *Int J Biol Sci*. 2018;14:1645-1657.
617 8. Nagaraju CK, Dries E, Gilbert G, Abdesselem M, Wang N, Amoni M, Driesen RB and
618 Sipido KR. Myofibroblast modulation of cardiac myocyte structure and function. *Sci Rep*.
619 2019;9:8879.
620 9. O'Hanlon R, Grasso A, Roughton M, Moon JC, Clark S, Wage R, Webb J, Kulkarni M,
621 Dawson D, Sulaibeekh L, Chandrasekaran B, Bucciarelli-Ducci C, Pasquale F, Cowie MR,
622 McKenna WJ, Sheppard MN, Elliott PM, Pennell DJ and Prasad SK. Prognostic significance of
623 myocardial fibrosis in hypertrophic cardiomyopathy. *J Am Coll Cardiol*. 2010;56:867-74.
624 10. Bruder O, Wagner A, Jensen CJ, Schneider S, Ong P, Kispert EM, Nassenstein K, Schlosser
625 T, Sabin GV, Sechtem U and Mahrholdt H. Myocardial scar visualized by cardiovascular
626 magnetic resonance imaging predicts major adverse events in patients with hypertrophic
627 cardiomyopathy. *J Am Coll Cardiol*. 2010;56:875-87.

628 11. Ellims AH, Iles LM, Ling LH, Hare JL, Kaye DM and Taylor AJ. Diffuse myocardial fibrosis in
629 hypertrophic cardiomyopathy can be identified by cardiovascular magnetic resonance, and is
630 associated with left ventricular diastolic dysfunction. *J Cardiovasc Magn Reson*. 2012;14:76.
631 12. Maron BJ and Longo DL. Clinical Course and Management of Hypertrophic
632 Cardiomyopathy. *New England Journal of Medicine*. 2018;379:655-668.
633 13. Tucker NR, Chaffin M, Fleming SJ, Hall AW, Parsons VA, Bedi KC, Jr., Akkad AD, Herndon
634 CN, Arduini A, Papangeli I, Roselli C, Aguet F, Choi SH, Ardlie KG, Babadi M, Margulies KB,
635 Stegmann CM and Ellinor PT. Transcriptional and Cellular Diversity of the Human Heart.
636 *Circulation*. 2020;142:466-482.
637 14. Litvinukova M, Talavera-Lopez C, Maatz H, Reichart D, Worth CL, Lindberg EL, Kanda M,
638 Polanski K, Heinig M, Lee M, Nadelmann ER, Roberts K, Tuck L, Fasouli ES, DeLaughter DM,
639 McDonough B, Wakimoto H, Gorham JM, Samari S, Mahbubani KT, Saeb-Parsy K, Patone G,
640 Boyle JJ, Zhang H, Zhang H, Viveiros A, Oudit GY, Bayraktar O, Seidman JG, Seidman CE, Noseda
641 M, Hubner N and Teichmann SA. Cells of the adult human heart. *Nature*. 2020;588:466-472.
642 15. Larson A and Chin MT. A method for cryopreservation and single nucleus RNA-
643 sequencing of normal adult human interventricular septum heart tissue reveals cellular
644 diversity and function. *BMC Med Genomics*. 2021;14:161.
645 16. Larson A, Codden CJ, Huggins GS, Rastegar H, Chen FY, Maron BJ, Rowin EJ, Maron MS
646 and Chin MT. Altered Intercellular Communication and Extracellular Matrix Signaling as a
647 Potential Disease Mechanism in Human Hypertrophic Cardiomyopathy. *medRxiv*.
648 2021:2021.12.18.21268004.
649 17. Zheng GX, Terry JM, Belgrader P, Ryvkin P, Bent ZW, Wilson R, Ziraldo SB, Wheeler TD,
650 McDermott GP, Zhu J, Gregory MT, Shuga J, Montesclaros L, Underwood JG, Masquelier DA,
651 Nishimura SY, Schnall-Levin M, Wyatt PW, Hindson CM, Bharadwaj R, Wong A, Ness KD, Beppu
652 LW, Deeg HJ, McFarland C, Loeb KR, Valente WJ, Ericson NG, Stevens EA, Radich JP, Mikkelsen
653 TS, Hindson BJ and Bielas JH. Massively parallel digital transcriptional profiling of single cells.
654 *Nat Commun*. 2017;8:14049.
655 18. Butler A, Hoffman P, Smibert P, Papalexi E and Satija R. Integrating single-cell
656 transcriptomic data across different conditions, technologies, and species. *Nat Biotechnol*.
657 2018;36:411-420.
658 19. Franzen O, Gan LM and Bjorkegren JLM. PanglaoDB: a web server for exploration of
659 mouse and human single-cell RNA sequencing data. *Database (Oxford)*. 2019;2019.
660 20. Falcon S and Gentleman R. Using GOstats to test gene lists for GO term association.
661 *Bioinformatics*. 2007;23:257-8.
662 21. Kramer A, Green J, Pollard J, Jr. and Tugendreich S. Causal analysis approaches in
663 Ingenuity Pathway Analysis. *Bioinformatics*. 2014;30:523-30.
664 22. Cao J, Spielmann M, Qiu X, Huang X, Ibrahim DM, Hill AJ, Zhang F, Mundlos S,
665 Christiansen L, Steemers FJ, Trapnell C and Shendure J. The single-cell transcriptional landscape
666 of mammalian organogenesis. *Nature*. 2019;566:496-502.
667 23. Skelly DA, Squiers GT, McLellan MA, Bolisetty MT, Robson P, Rosenthal NA and Pinto AR.
668 Single-Cell Transcriptional Profiling Reveals Cellular Diversity and Intercommunication in the
669 Mouse Heart. *Cell Rep*. 2018;22:600-610.
670 24. Larson A, Codden CJ, Huggins GS, Rastegar H, Chen FY, Maron BJ, Rowin EJ, Maron MS
671 and Chin MT. Altered Intercellular Communication And Extracellular Matrix Signaling As A

672 Disease Mechanism In Human Hypertrophic Cardiomyopathy. *Preprint (version 1) available at*
673 *https://papersssrncom/sol3/paperscfm?abstract_id=3965237*. 2021.
674 25. Ramilowski JA, Goldberg T, Harshbarger J, Kloppmann E, Lizio M, Satagopam VP, Itoh M,
675 Kawaji H, Carninci P, Rost B and Forrest AR. A draft network of ligand-receptor-mediated
676 multicellular signalling in human. *Nat Commun*. 2015;6:7866.
677 26. Shao X, Liao J, Li C, Lu X, Cheng J and Fan X. CellTalkDB: a manually curated database of
678 ligand-receptor interactions in humans and mice. *Brief Bioinform*. 2020.
679 27. Chou C and Chin MT. Pathogenic Mechanisms of Hypertrophic Cardiomyopathy beyond
680 Sarcomere Dysfunction. *Int J Mol Sci*. 2021;22:8933.
681 28. Liu X, Shi GP and Guo J. Innate Immune Cells in Pressure Overload-Induced Cardiac
682 Hypertrophy and Remodeling. *Front Cell Dev Biol*. 2021;9:659666.
683 29. Wang H, Kwak D, Fassett J, Liu X, Yao W, Weng X, Xu X, Xu Y, Bache RJ, Mueller DL and
684 Chen Y. Role of bone marrow-derived CD11c(+) dendritic cells in systolic overload-induced left
685 ventricular inflammation, fibrosis and hypertrophy. *Basic Res Cardiol*. 2017;112:25.
686 30. Athanassopoulos P, Balk AH, Vaessen LM, Caliskan K, Takkenberg JJ, Weimar W and
687 Bogers AJ. Blood dendritic cell levels and phenotypic characteristics in relation to etiology of
688 end-stage heart failure: implications for dilated cardiomyopathy. *Int J Cardiol*. 2009;131:246-56.
689 31. Swetman Andersen CA, Handley M, Pollara G, Ridley AJ, Katz DR and Chain BM. beta1-
690 Integrins determine the dendritic morphology which enhances DC-SIGN-mediated particle
691 capture by dendritic cells. *Int Immunol*. 2006;18:1295-303.
692 32. Yokota-Nakatsuma A, Ohoka Y, Takeuchi H, Song SY and Iwata M. Beta 1-integrin
693 ligation and TLR ligation enhance GM-CSF-induced ALDH1A2 expression in dendritic cells, but
694 differentially regulate their anti-inflammatory properties. *Sci Rep*. 2016;6:37914.
695 33. Krishnaswami SR, Grindberg RV, Novotny M, Venepally P, Lacar B, Bhutani K, Linker SB,
696 Pham S, Erwin JA, Miller JA, Hodge R, McCarthy JK, Kelder M, McCorrison J, Aevermann BD,
697 Fuertes FD, Scheuermann RH, Lee J, Lein ES, Schork N, McConnell MJ, Gage FH and Lasken RS.
698 Using single nuclei for RNA-seq to capture the transcriptome of postmortem neurons. *Nat*
699 *Protoc*. 2016;11:499-524.
700 34. Zappia L and Oshlack A. Clustering trees: a visualization for evaluating clusterings at
701 multiple resolutions. *Gigascience*. 2018;7.
702 35. McLellan MA, Skelly DA, Dona MSI, Squiers GT, Farrugia GE, Gaynor TL, Cohen CD,
703 Pandey R, Diep H, Vinh A, Rosenthal NA and Pinto AR. High-Resolution Transcriptomic Profiling
704 of the Heart During Chronic Stress Reveals Cellular Drivers of Cardiac Fibrosis and Hypertrophy.
705 *Circulation*. 2020;142:1448-1463.
706 36. UniProt C. UniProt: the universal protein knowledgebase in 2021. *Nucleic Acids Res*.
707 2021;49:D480-D489.
708 37. Csardi G and Nepusz T. The igraph software package for complex network research.
709 *InterJournal*. 2006;Complex Systems:1695.
710 38. Yu G, Wang LG, Han Y and He QY. clusterProfiler: an R package for comparing biological
711 themes among gene clusters. *OMICS*. 2012;16:284-7.
712

713

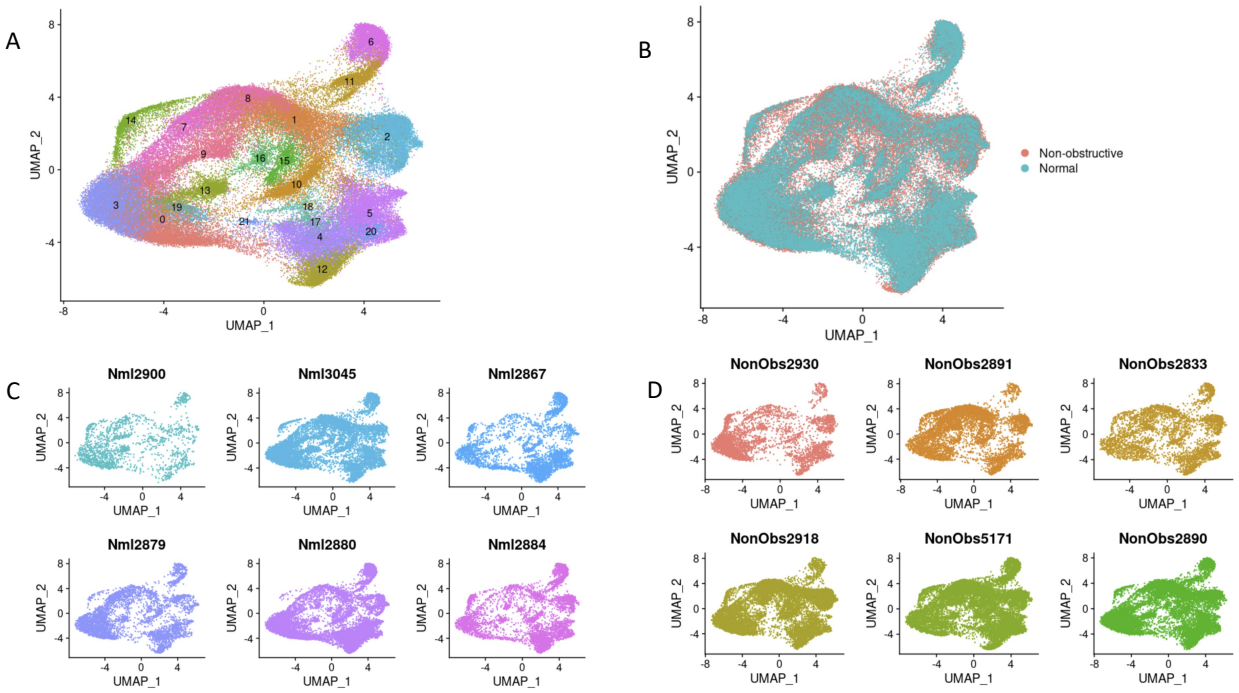

714

715

716 **Fig. 1. Single nuclei RNA-seq of Normal and HCM IVS Tissue Reveals Cellular Diversity but No**

717 **HCM-associated Cell Types. A**. UMAP plot of 22 distinct cell clusters identified in the combined

718 Normal and nonobstructive HCM dataset. **B**. Separating the cell clusters by condition does not

719 identify HCM-specific cell types. **C**. Cluster distribution in each Normal sample. D. Cluster

720 distribution in each nonobstructive HCM sample.

721

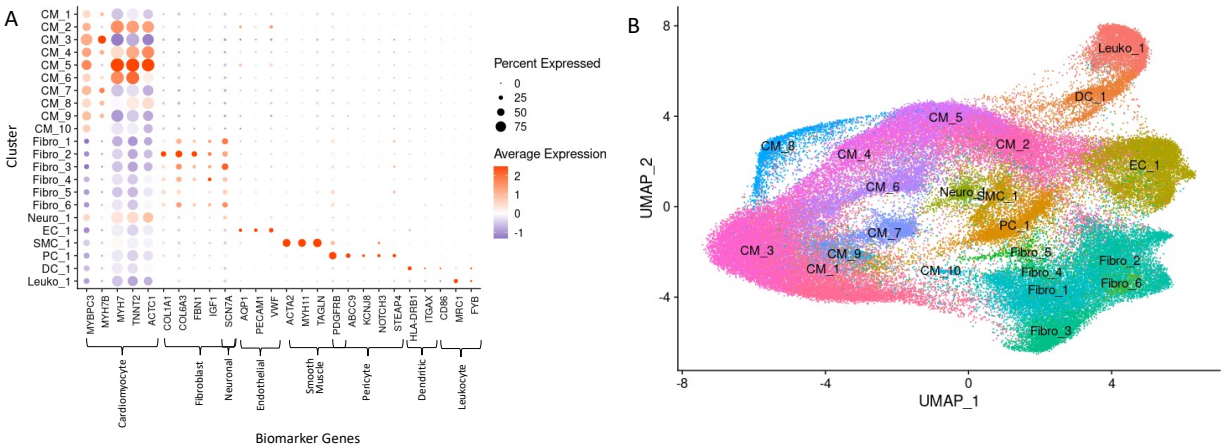

722

723

724 **Fig. 2. Biomarker Expression and Cell Identification Assignments for each Cluster. A**.

725 Biomarkers used to assign cell identity and their relative expression in each cluster. **B**. UMAP

726 plot of IVS tissue clusters with cell assignment labels.

727

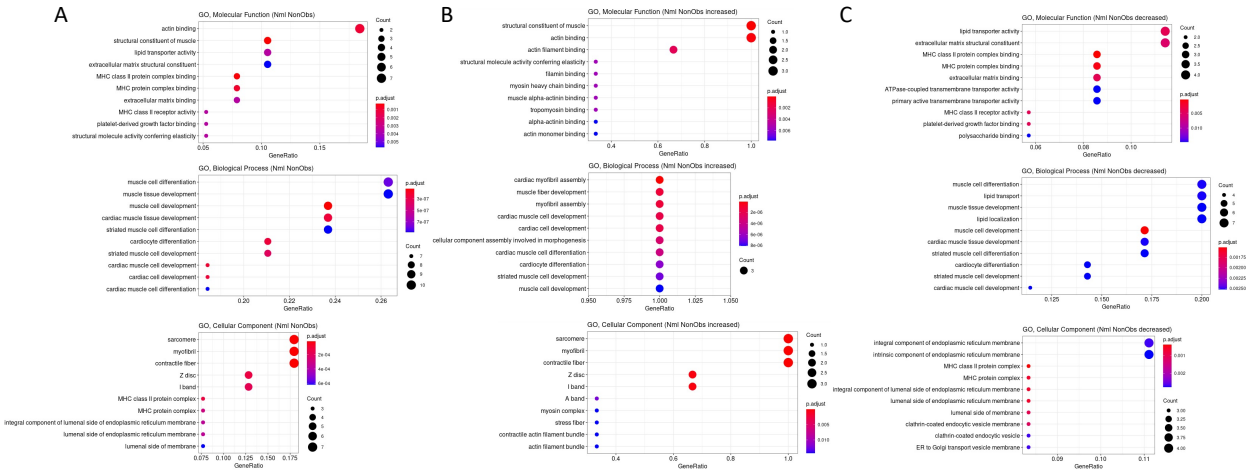

Fig. 3. Gene Ontology Enrichment Analysis of Differentially Expressed Genes in nonobstructive HCM. **A**. GO enrichment analysis of all differentially expressed genes in HCM from Table 3. **B**. GO enrichment analysis of Table 3 genes increased in nonobstructive HCM. **C**. GO enrichment analysis of Table 3 genes decreased in nonobstructive HCM.

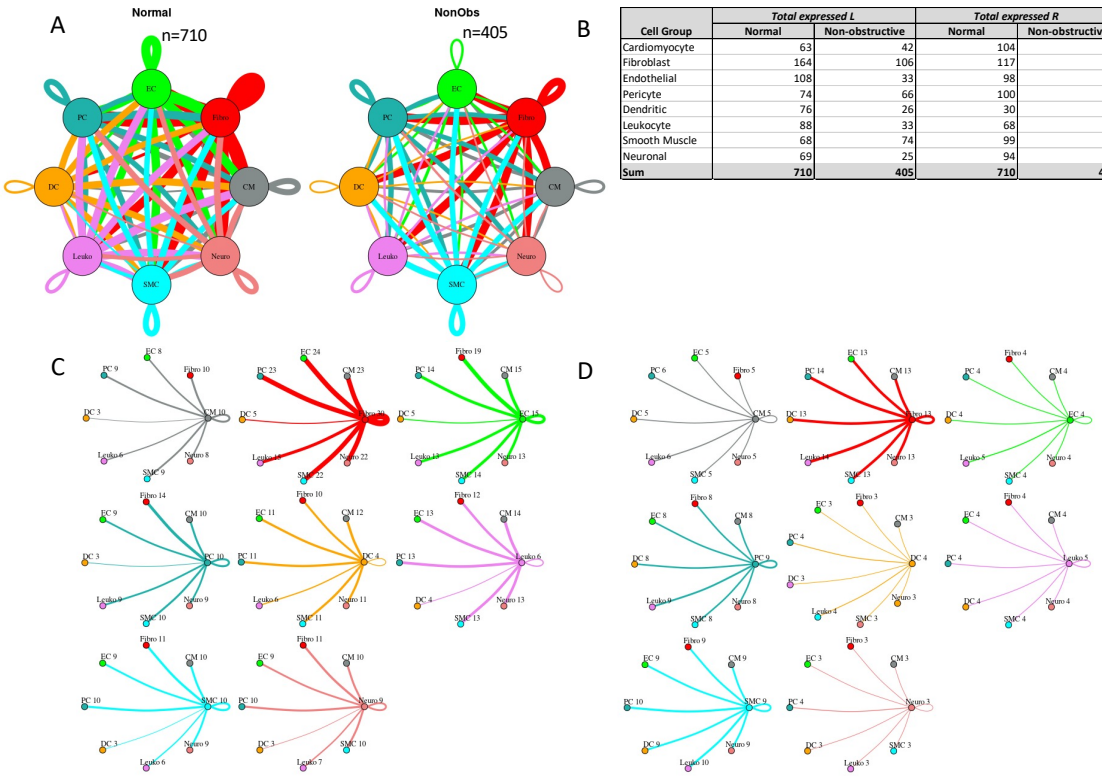

Cell Group	Total expressed L		Total expressed R	
	Normal	Non-obstructive	Normal	Non-obstructive
Cardiomyocyte	63	42	104	49
Fibroblast	164	106	117	49
Endothelial	108	33	98	49
Pericyte	74	66	100	55
Dendritic	76	26	30	49
Leukocyte	88	33	68	56
Smooth Muscle	68	74	99	49
Neuronal	69	25	94	49
Sum	**710**	**405**	**710**	**405**

Fig. 4. Intercellular communication networks are reduced in nonobstructive HCM. **A**. Cell-cell communication networks between cardiac cell types in normal control (left) and nonobstructive HCM (right) conditions. Line color indicates ligand broadcast by the cell population with the same color. Lines connect to cell types which expressed cognate receptors. Line thickness is proportional to the number of uniquely expressed ligand-receptor pairs. Loops indicates communication within a cell type. **B**. Quantity of ligands and receptors in expressed ligand-receptor pairs described by cell type and condition (Normal or nonobstructive HCM). **C**., **D**. Cell-cell communication networks broken down by cell type in normal control (**C**) and nonobstructive HCM (**D**) conditions. Figure formatting follows panel A. Numbers indicate the quantity of uniquely expressed ligand-receptor pairs between the broadcasting cell type (expressing ligand) and receiving cell type (expressing receptor).

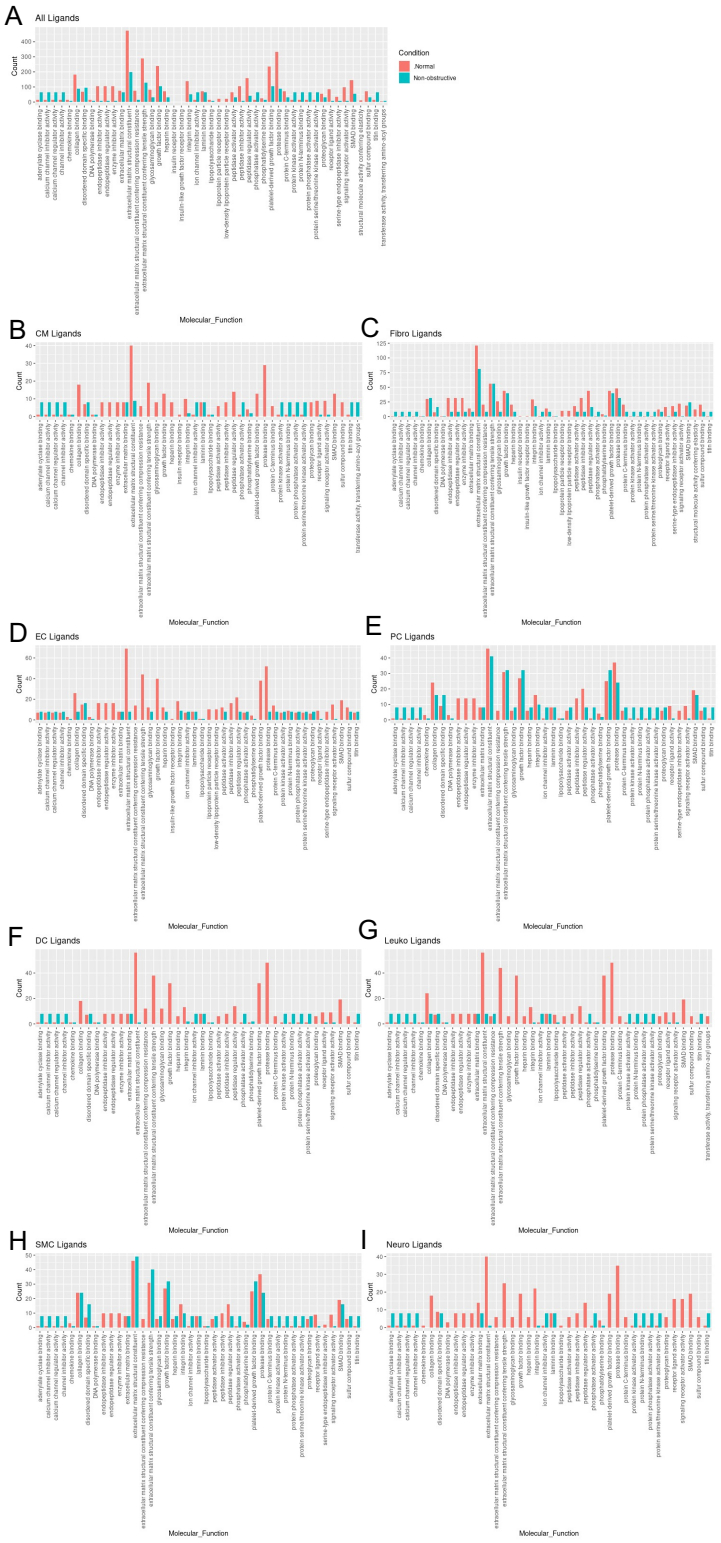
A
All Ligands
Condition
Normal
Non-obstructive
Count
Molecular_Function
B
CM Ligands
C
Fibro Ligands
D
EC Ligands
E
PC Ligands
F
DC Ligands
G
Leuko Ligands
H
SMC Ligands
I
Neuro Ligands

747

748

749 **Fig. 5. Bar plot representing the total count of ligands (in expressed ligand-receptor pairs)**

750 **associated with different cellular processes in Normal and nonobstructive HCM IVS Cells.** Bar

751 color distinguishes ligand count in normal or nonobstructive HCM conditions. **A**. Comparison of

752 molecular functions across all cell types. **B**. Comparison in cardiomyocytes. **C**. Fibroblasts. **D**.

753 Endothelial Cells. **E**. Pericytes. **F.** Dendritic Cells. **G.** Leukocytes. **H**. Smooth Muscle Cells. **I**.

754 Neurons.

755

Fig. 6. Bar plot representing the total count of receptors (in expressed ligand-receptor pairs) associated with different cellular processes in Normal and nonobstructive HCM IVS Cells. Bar

760 color distinguishes receptor count in normal or nonobstructive HCM conditions. **A**. Comparison

761 of molecular functions across all cell types. **B**. Comparison in cardiomyocytes. **C**. Fibroblasts. **D**.

762 Endothelial Cells. **E**. Pericytes. **F.** Dendritic Cells. **G.** Leukocytes. **H**. Smooth Muscle Cells. **I**.

763 Neurons.

764

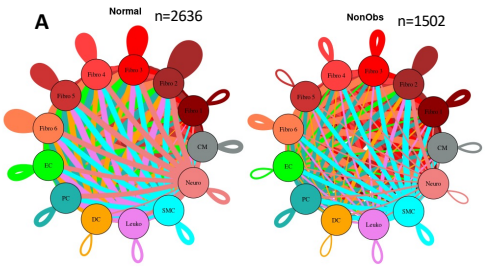

B

Cell Group	Total expressed L		Total expressed R	
	Normal	Non-obstructive	Normal	Non-obstructive
Cardiomyocyte	109	72	213	109
Fibroblast 1	239	163	95	109
Fibroblast 2	401	256	286	171
Fibroblast 3	266	188	252	109
Fibroblast 4	242	135	252	109
Fibroblast 5	241	58	275	109
Fibroblast 6	299	191	252	109
Endothelial	198	58	209	110
Pericyte	140	110	211	120
Dendritic	122	46	54	109
Leukocyte	142	57	133	120
Smooth Muscle	118	123	205	109
Neuronal	119	45	199	109
Sum	**2636**	**1502**	**2636**	**1502**

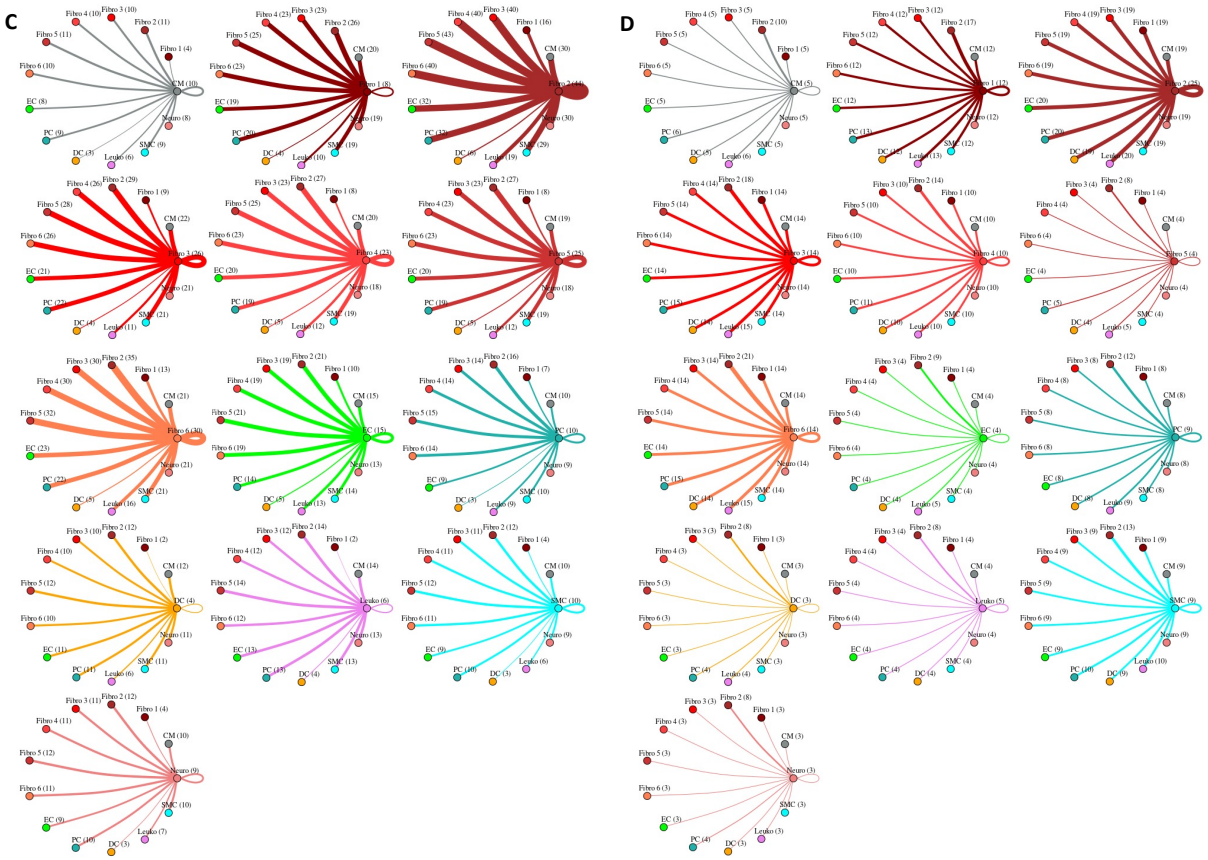

Fig. 7. Cell-cell communication networks between fibroblast subtypes and other heart cells in normal control and nonobstructive HCM conditions. A. Comparison of Normal (left) and nonobstructive HCM (right) communication networks. Line color indicates ligand broadcast by the cell population with the same color. Lines connect to cell types which expressed cognate receptors. Line thickness is proportional to the number of uniquely expressed ligand-receptor pairs. Loops indicates communication within a cell type. **B.** Quantity of ligands and receptors in

773 expressed ligand-receptor pairs described by cell type and condition (Normal or nonobstructive

774 HCM). **C, D.** Cell-cell communication networks broken down by cell type and fibroblast cluster

775 in normal control (**C**) and nonobstructive HCM (**D**) conditions. Figure formatting follows panel A.

776 Numbers indicate the quantity of uniquely expressed ligand-receptor pairs between the

777 broadcasting cell type (expressing ligand) and receiving cell type (expressing receptor).

778

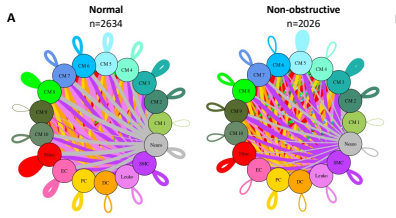

B

Cell Group	Total expressed L		Total expressed R	
	Normal	Non-obstructive	Normal	Non-obstructive
Cardiomyocyte 1	47	49	40	41
Cardiomyocyte 2	145	174	164	106
Cardiomyocyte 3	168	130	220	229
Cardiomyocyte 4	97	88	203	103
Cardiomyocyte 5	194	266	169	144
Cardiomyocyte 6	113	83	183	106
Cardiomyocyte 7	114	99	201	154
Cardiomyocyte 8	219	124	202	129
Cardiomyocyte 9	61	83	40	154
Cardiomyocyte 10	104	81	166	106
Fibroblast	338	231	202	103
Endothelial	229	81	164	104
Pericyte	154	143	174	118
Dendritic	168	73	55	105
Leukocyte	194	77	118	118
Smooth Muscle	144	173	173	103
Neuronal	145	71	160	103
Sum	**2634**	**2026**	**2634**	**2026**

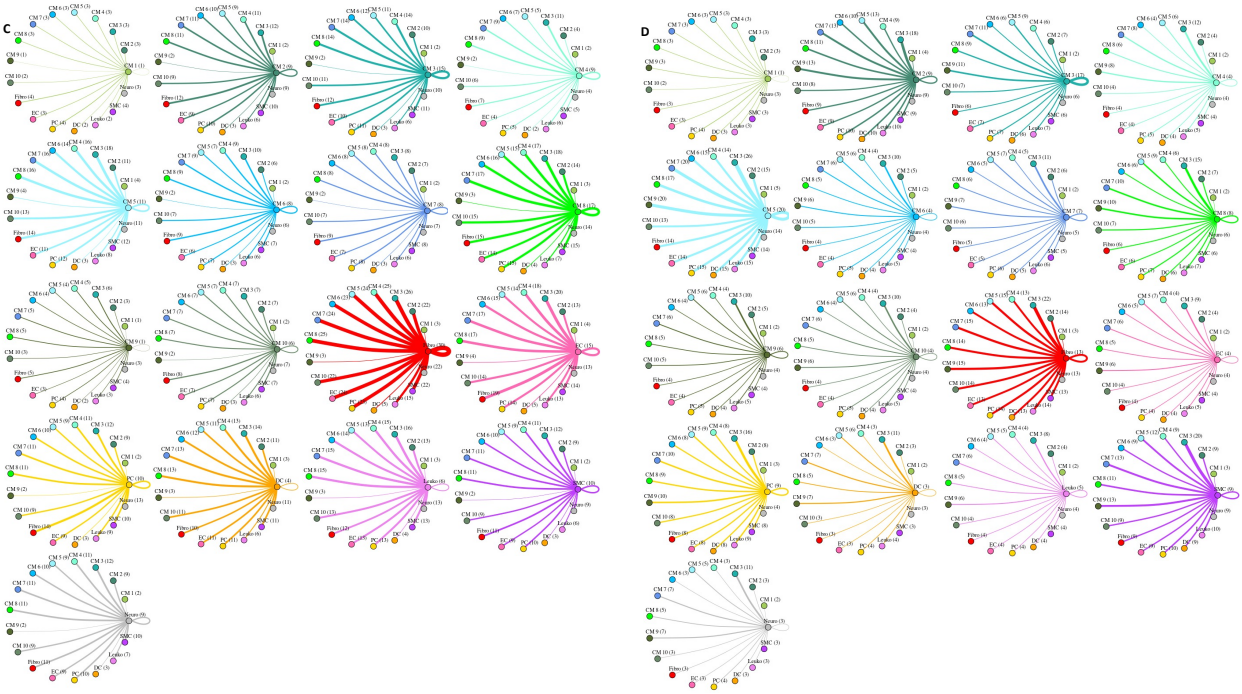

Fig. 8. Cell-cell communication networks between cardiomyocyte subtypes and other heart cells in normal control and nonobstructive HCM conditions. A. Comparison of Normal (left) and nonobstructive HCM (right) communication networks. Line color indicates ligand broadcast by the cell population with the same color. Lines connect to cell types which expressed cognate receptors. Line thickness is proportional to the number of uniquely expressed ligand-receptor pairs. Loops indicates communication within a cell type. **B.** Quantity of ligands and receptors in expressed ligand-receptor pairs described by cell type and condition (Normal or nonobstructive HCM). **C, D.** Cell-cell communication networks broken down by cell type and cardiomyocyte cluster in normal control (**C**) and nonobstructive HCM (**D**) conditions. Figure formatting follows

790 panel A. Numbers indicate the quantity of uniquely expressed ligand-receptor pairs between

791 the broadcasting cell type (expressing ligand) and receiving cell type (expressing receptor).

792

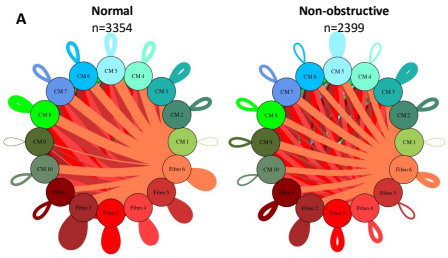

B

Cell Group	Total expressed L		Total expressed R	
	Normal	Non-obstructive	Normal	Non-obstructive
Cardiomyocyte 1	47	45	40	44
Cardiomyocyte 2	152	167	201	142
Cardiomyocyte 3	171	124	256	263
Cardiomyocyte 4	104	86	241	132
Cardiomyocyte 5	202	256	217	171
Cardiomyocyte 6	121	81	221	134
Cardiomyocyte 7	117	96	237	179
Cardiomyocyte 8	217	121	242	156
Cardiomyocyte 9	65	80	40	179
Cardiomyocyte 10	104	79	205	138
Fibroblast 1	298	206	104	132
Fibroblast 2	481	325	289	201
Fibroblast 3	330	237	260	132
Fibroblast 4	299	171	260	132
Fibroblast 5	293	79	281	132
Fibroblast 6	353	246	260	132
Sum	**3354**	**2399**	**3354**	**2399**

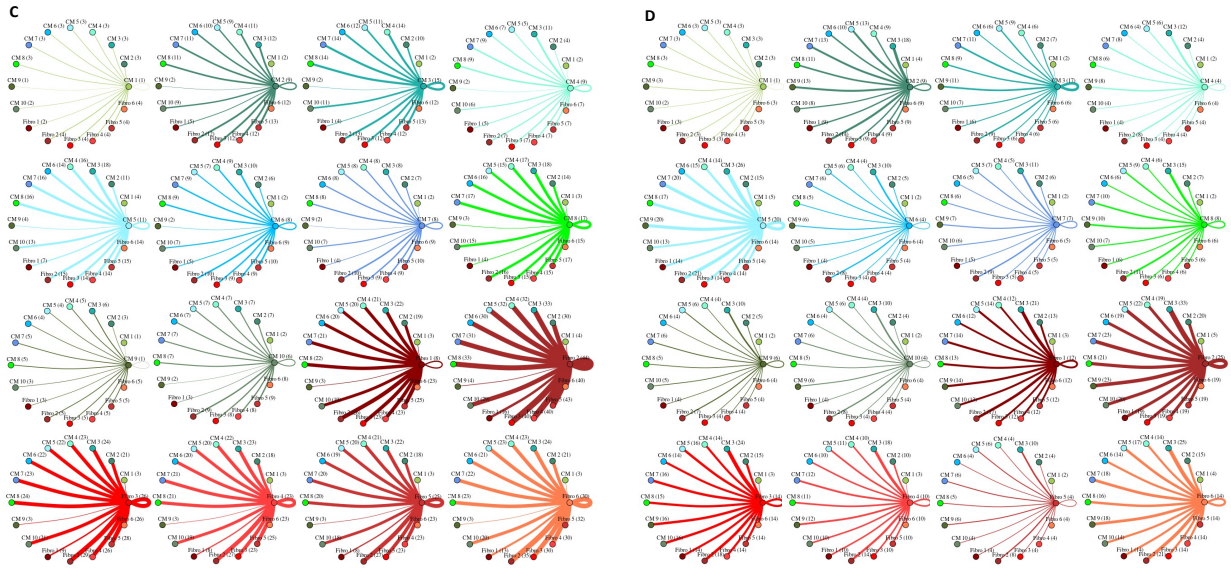

Fig. 9. Cell-cell communication networks between cardiac fibroblast and cardiomyocyte subtypes in normal control and HCM conditions. A. Overall communication network between cardiomyocytes and fibroblasts. Line color indicates ligand broadcast by the cell population with the same color. Lines connect to cell types which expressed cognate receptors. Line thickness is proportional to the number of uniquely expressed ligand-receptor pairs. Loops indicates communication within a cell type. **B.** Quantity of ligands and receptors in expressed ligand-receptor pairs described by cell type and condition (Normal or nonobstructive HCM). **C, D.** Cell-cell communication networks broken down by cardiomyocyte cluster and fibroblast cluster in normal control (**C**) and nonobstructive HCM (**D**) conditions. Figure formatting follows panel A.

804 Numbers indicate the quantity of uniquely expressed ligand-receptor pairs between the

805 broadcasting cell type (expressing ligand) and receiving cell type (expressing receptor).

806

807 Table 1. HCM Patient Characteristics

Patient	2833	2890	2891	2918	2930	5171
Demographics						
age at transplant	21-25	61-65	46-50	61-65	36-40	66-70
female	yes	yes	no	yes	yes	yes
nyha class>3	yes	yes	yes	yes	yes	yes
Med Hx						
Prior AF	no	yes	yes	yes	yes	no
Prior VT/VF	yes	no	no	no	no	yes
Prior NS VT	no	no	no	no	no	yes
Prior syncope	yes	no	yes	no	no	no
Fam Hx SCD	no	no	yes	yes	no	yes
Fam Hx HCM	no	no	yes	yes	yes	yes
Comorbidities	none	HTN, HLD, COPD, DM2, CHB, OA, prior myectomy	OSA, Sarcoidosis	CAD, hypothyroidism	hypothyroidism, apical hypertrophy	asthma, HLD, apical aneurysm
Meds						
beta blocker	yes	yes	no	yes	no	yes
calcium channel blocker	no	no	no	no	no	no
ACE or ARB	no	no	no	yes	no	yes
Diuretic Use	yes	yes	yes	yes	yes	yes
loop diuretic	yes	yes	yes	yes	yes	yes
thiazide	no	yes	yes	no	no	yes
potassium sparing	yes	yes	yes	yes	yes	yes
disopyramide	no	no	no	no	no	no
amiodarone	no	no	no	no	yes	no
milrinone	yes	yes	yes	yes	no	yes
dofetilide	no	no	yes	no	no	no
ICD	yes	yes	yes	yes	yes	yes
Physiological measurements						
LA size (mm)	47	37	36	64	33	51
systolic blood pressure	95	103	120	87	99	130
diastolic blood pressure	57	56	54	66	49	67
IVS thickness (mm)	26	11 (prior myectomy)	13	18	9.5	9
Posterior wall thickness	20	0.88	13	16	7.7	9
LVEF (%)	15-20	65	60	45	65	25-30
LVEDD (mm)	51	46	45	41	45	57
LVESD (m)	49	29	28	35	49	41
MR	mild	trace	no	trace	mild	mild
LGE on MRI	24%	none	ND	ND	none	ND
Pathogenic HCM Variant	NF	NF	MYH7	NF	NF	MYH7

808
809

810 Table 2. Organ Donor Characteristics

Donor	2867	2879	2880	2884	2900	3045
age	21-25	56-60	41-45	41-45	46-50	66-70
female	yes	no	no	yes	no	yes
cause of death	asphyxiation	CVA	head trauma	seizure	overdose	CVA
cardiac risk factors	none	none	none	HTN, Tobacco	none	HLD
CAD	not assessed	20% LAD	not assessed	not assessed	not assessed	not assessed
LVEF	81%	60%	not assessed	55%	not assessed	70%
Medications	antidepressants, OCP	none	unknown	unknown	unknown	statin, levothyroxine

811

812

813 Table 3. Differentially Expressed Genes in Nonobstructive HCM with Pronounced Changes in

814 Spatial Expression

	Gene of Interest	Affected Cell Group	Expression in Non-obstructive HCM	Established HCM Gene
1	ABCA10	Cardiomyocyte, Fibroblast	Decreased	
2	ABCA6	Cardiomyocyte	Decreased	
3	ABCA8	Cardiomyocyte	Decreased	
4	AC010680.1	Cardiomyocyte	Increased	
5	AC010680.5	Cardiomyocyte	Increased	
6	ADH1B	Cardiomyocyte	Decreased	
7	AGT	Endothelial, Pericyte	Decreased	
8	C1R	Fibroblast	Decreased	
9	C1S	Fibroblast	Decreased	
10	CCL21	Endothelial	Decreased	
11	CD74	Dendritic	Decreased	
12	COL1A2	Neuronal	Decreased	
13	CPE	Pericyte	Decreased	
14	EMC10	Cardiomyocyte	Decreased	
15	FABP4	Endothelial, Pericyte	Decreased	
16	FBLN2	Fibroblast	Decreased	
17	HES1	Fibroblast	Decreased	
18	HES4	Smooth Muscle	Decreased	
19	HLA-DRA	Dendritic	Decreased	
20	HLA-DRB1	Dendritic	Decreased	
21	IGFBP5	Endothelial	Decreased	
22	MEG3	Cardiomyocyte, Fibroblast	Decreased	
23	MMRN1	Endothelial	Decreased	
24	MS4A6A	Dendritic	Decreased	
25	MYH7	Neuronal	Decreased	Yes
26	MYH7B	Cardiomyocyte	Decreased	
27	MYL2	Cardiomyocyte	Increased	Yes
28	NDUFA4L2	Pericyte	Decreased	
29	NEBL	Cardiomyocyte	Increased	
30	NPPB	Cardiomyocyte	Decreased	
31	PDGFRB	Pericyte, Smooth Muscle	Decreased	
32	PLA2G2A	Cardiomyocyte	Decreased	
33	PTGIR	Cardiomyocyte	Decreased	
34	RP11-394O4.5	Smooth Muscle	Decreased	
35	RP11-532N4.2	Cardiomyocyte	Decreased	
36	SAT1	Dendritic	Decreased	
37	SLC8A1	Cardiomyocyte	Decreased	
38	SORBS2	Cardiomyocyte	Decreased	
39	SPARC	Neuronal	Decreased	
40	SPP1	Neuronal	Decreased	
41	TFPI	Endothelial	Decreased	
42	TMSB4X	Endothelial	Decreased	
43	TNNT2	Dendritic, Neuronal	Decreased	Yes
44	TTN	Neuronal	Increased	

815